SIAM J. Applied Dynamical Systems
Vol. 13, No. 3, pp. 1152–1167

A Bifurcation Approach to the Synchronization of Coupled Van der Pol Oscillators*

Rubén Gustavo Paccosi†, Alejandra Figliola†, and Jorge Galán-Vioque‡

Abstract. We undertake a bifurcation analysis of a velocity coupled system of two classical nonidentical Van der Pol oscillators to understand the appearance and structure of 1:k parameter regions with synchronized states as we vary the coupling and the frequency mismatch. These regions include multistability of solutions and are formed by classical tongues bordered by curves of limit point bifurcation of periodic orbits with an isola structure and an additional subregion surrounded by curves of torus bifurcations and a curve characterized by a geometrical tangency condition. Symmetry arguments explain the difference between the even and odd k cases.

Key words. oscillator synchronization, bifurcation of periodic orbits, numerical continuation, synchronization tongues

AMS subject classifications. 34D06, 34C15, 37M20

DOI. 10.1137/130926602

1. Introduction.

First recognized in 1665 by Huygens, who observed two mechanically coupled clocks [12], synchronization phenomena are ubiquitous in science, nature, engineering, and social life. Systems as diverse as singing crickets, cardiac pacemakers, firing neurons, and applauding audiences exhibit a tendency to operate in synchrony [23]. Loosely speaking, synchronization could be defined as an adjustment of rhythms of oscillating objects due to their weak interaction. It is a universal phenomenon and can be understood within a common framework based on modern nonlinear dynamics [3, 10]. A rather mathematical but unifying definition of the different types of synchronization can be found in [5].

The Van der Pol oscillator [34, 35] is the canonical example of a planar limit cycle. It has been extensively studied by the dynamical systems community from both the theoretical and the numerical point of view and is a necessary character in any textbook on dynamical systems [10, 18, 30].

The applications of the Van der Pol oscillator start with the classical work by Van der Pol himself [36], who applied it to an electrical model of the heart [36]. Since then, it has been used, for instance, in a mathematical model based on interconnected relaxation oscillators for the slow wave electrical circuit of the gastrointestinal tract [20], in a heuristic model of neuron interactions [14], in the modeling of circadian rhythms [26], in the rhythm synchronization in

*Received by the editors June 26, 2013; accepted for publication (in revised form) by H. Osinga April 2, 2014; published electronically July 31, 2014. This research was supported by Spanish grants MICINN MTM2009-07849 and MINECO MTM2012-31821.
http://www.siam.org/journals/siads/13-3/92660.html
†Instituto del Desarrollo Humano, Universidad Nacional de General Sarmiento, 1613 Los Polvorines, Buenos Aires, Argentina (gpaccosi@yahoo.com, alejandra.figliola@gmail.com).
‡Matemática Aplicada II, Escuela Superior de Ingeniería, Universidad de Sevilla, and Instituto de Matemáticas de la Universidad de Sevilla, Sevilla 41092, Spain (jgv@us.es).

a model of the heartbeat [8], in synchronization of electromechanical devices [39], in control of biped locomotion [13], and as a simplified model of the self-excited vibrations in turbomachine blades [4].

It is well known that the forced case exhibits complex dynamical behavior, and the coupled version has become the basic model of nonlinear dynamical systems undergoing mutual synchronization.

The phenomena of synchronization, oscillator suppression, and total oscillator death are universal phenomena that have already been studied for other systems.

Vance and Ross [37], Aronson, Ermentrout, and Kopell [2], and Taylor and Kevrekidis [33] have established the generic bifurcation structure for the transition from quasi periodicity and synchronization to the regime of oscillator suppression as the coupling (or forcing) increases. They have shown, for instance, how the 1:1 resonance tongue is bounded at the top by a saddle-node bifurcation curve, how the 1:2 tongue ends with one or more period-doubling bifurcation curves, and how the 1:3 tongue ends with a loop of its delineating saddle-node bifurcation curve around the so-called period-3 resonance point on the torus bifurcation curve. This is the curve that, between the resonance tongues, marks the transition from quasi periodicity to oscillator suppression. For weak resonances, the delineating saddle-node bifurcation curves are tangent to the torus bifurcation curve in their respective resonance points.

A similar result was obtained by Sturis et al. [31] in a study of the response of the ultradian oscillations in human insulin secretion to an oscillatory intravenous glucose infusion. It may also be worth noting that similar phenomena have been observed in a spatially extended electronic oscillator [21].

Taylor and Kevrekidis [32] and Ermentrout [9] have considered the transition from oscillator suppression to total oscillator death. They have observed, for instance, that two different Hopf bifurcations of the equilibrium point may be involved and that a small region of torus dynamics may develop from the point of intersection between these two Hopf bifurcation curves.

The idea of coupling several Van der Pol oscillators has been extensively used in the literature and started with, to the best of our knowledge, an analytical treatment of two coupled Van der Pol oscillators in [1]. The corresponding bifurcation behavior was studied in [11] and [29]. Two weakly coupled identical and detuned Van der Pol oscillators analyzed by means of perturbative and topological methods can be found in [24]. An indirect coupling via a bath was analyzed in [6], and multistability of solutions was found in [22]. Natural extensions of the model by including delay or a nonautonomous term can be found in [19] and [17], respectively.

A generic trajectory in the case of two nonidentical oscillators would be quasi-periodic, and the invariant tori and their bifurcation should play a preeminent role in the description of the global dynamics. For an extensive treatment of tori continuation and their bifurcation and a review of the related works, we refer the reader to [28] and [25].

In a recent work [16] the case of nonidentical velocity coupled Van der Pol systems was numerically investigated, and a so-called *broadband synchronization* region was identified in which the two oscillators perform periodic orbits with commensurate periods. More precisely, by means of an appropriate Poincaré three-dimensional section they found that, for an unbounded region in the frequency mismatch parameter and moderate values of the coupling,

one of the subsystems performed one full revolution, while the other completed k full revolutions; i.e., the 1:k synchronized state. We will take this statement as a working definition of synchronization that implies additionally that the solution under consideration is *periodic* and *stable*. We are aware that this is not the only definition of synchronization [5], but it is the one considered by the authors of [16], whose results are under analysis. For instance, we do not require that the flow of the orbit lies on the surface of a torus. This may lead to an interpretation of our results which seems to be in conflict with previous work. We will recall this fact whenever appropriate.

The well-known Arnold tongues that emanate from the zero coupling limit act as bridges toward the broad synchronized region and appear in an ordered and monotonic way in k as we increase the frequency mismatch parameter. In [16] Kuznetsov and Roman identified, among other features, the 1:1, 1:3, and 1:5 synchronization tongues that appear with decreasing width as the classical theory predicts, but did not analyze the case of even k values. In addition, the border and structure of the upper part of the tongues that overlaps with the main 1:1 broadband region were designated as *degraded top* for their geometrical shape and were not completely explained.

In this paper we undertake a bifurcation analysis of this velocity coupled system of two classical nonidentical Van der Pol oscillators to understand the appearance and structure of 1:k parameter regions with synchronized states as we vary the coupling and the frequency mismatch. We will show that these regions include multistability of solutions and are formed by classical tongues bordered by curves of limit point bifurcations of periodic orbits with an isola structure and an additional area surrounded by curves of torus bifurcations and a curve characterized by a geometrical tangency condition. We will also show that symmetry arguments explain the difference between the even and odd k cases.

2. The model. The model under study is formed by two classical Van der Pol oscillators represented by the following system of second order differential equations:

$$\begin{cases} \ddot{x} - (1 + \lambda - x^2)\dot{x} + x = \mu(\dot{y} - \dot{x}), \\ \ddot{y} - (1 - y^2)\dot{y} + (1 + \delta)y = \mu(\dot{x} - \dot{y}). \end{cases} \tag{2.1}$$

For the sake of simplicity and to compare with the results of [16] we have considered only a dissipative coupling (velocity dependent) instead of a reactive one (position dependent) or a combination of both. An interesting and recent review on the different coupling options, including a mixing of positions and velocity (conjugate coupling), can be found in [27].

The parameter λ in the first equation controls the appearance of the Hopf bifurcation, the parameter δ is the frequency mismatch, μ parametrizes the dissipative coupling, and, as usual, the dot denotes the time derivative.

In the absence of coupling, the two oscillators have a stable limit cycle with, in general, different frequencies. In addition, it is intuitive to think that, for almost identical oscillators (small λ and δ), a moderate amount of coupling will bring the system into a synchronized state. The question of interest is to understand what happens for arbitrary values of the parameters, i.e., for which value of the parameters these two oscillatory subsystems enter a synchronized state.

The authors of [16] undertook an extensive numerical investigation of the parameter dependence of the solutions of (2.1) by scanning a fine grid in the δ-μ parameter plane for fixed λ.

They also performed some asymptotic expansions to understand the structure of the solutions. They identified regions where no oscillations were present (the so-called death of oscillation region), as well as regions where the two subsystems were oscillating in a 1:1 synchronized state. More interestingly, by means of a three-dimensional Poincaré section they were able to detect parameter values for which one of the subsystems performed k complete oscillations, whereas the other did only one, a 1:k synchronized state. Furthermore, they completed the analysis by repeating the computation for different values of λ and by monitoring the evolution of the different regions.

However, for each pixel in the δ-μ parameter representations of the solutions of equations (2.1) [16, eqs. (1)], only one state was assigned to the system, precluding the possibility of multistability, and the transition from one state to another was not completely explained.

We will see that a bifurcation-based approach based on continuation of solutions provides a complementary point of view that clarifies the representation of the solutions and helps in completing the puzzle, in particular, in identifying the geometrical mechanism in the upper part of the synchronization tongues (the so-called degraded top region). As we will see later (section 3.2), Kuznetsov and Roman overlooked some observable structures associated with even values of k.

3. Results. The basic tool for our study has been the continuation of the unique equilibrium point of the system, which turns out to be the origin. The simplicity of the model allows some analytical treatment so that the curves of the equilibria bifurcation can be worked out with standard linear algebra techniques.

In general terms, for any given value of λ, the equilibrium is stable for large values of δ and large values of μ; i.e., when the two subsystems have very different values of frequencies or the coupling is very strong, any oscillatory solutions are suppressed.

As we decrease any of these parameters, the equilibrium loses its stability via a Hopf bifurcation where a pair of complex conjugate eigenvalues crosses the imaginary access with nonzero velocity and a limit cycle is born. This first bifurcation can be fully characterized by computing analytically the first Lyapunov coefficient which turns out to be negative, indicating that the bifurcation is supercritical and, consequently, the emanating periodic orbit is stable. This Hopf bifurcation condition can be traced in two parameters (δ-μ) to identify the onset of synchronized states and is presented in Figure 1 for $\lambda = 0.25$. It is clear from our definition in section 1 that any stable periodic orbit corresponds to a synchronized solution, because the system is oscillating in a periodic and stable condition. A geometrical analysis of the orbit will tell us whether it is a 1:k synchronized state or something more exotic.

By further decreasing the value of μ, the origin undergoes a second Hopf bifurcation in which the other pair of complex conjugate eigenvalues crosses the imaginary axis, meaning that the already unstable equilibrium becomes doubly unstable and a second family of unstable periodic solutions is born. According to our results, this second bifurcation has no direct influence in the synchronization phenomenon.

This second curve of Hopf bifurcation in the δ-μ plane is shown in Figure 1 and does not separate regions of observable different dynamical behavior because the equilibrium before and after the crossing was already unstable. We should remark that the case $\lambda = 0$ is a special case where the two Hopf curves coincide (in fact, are equal to a horizontal segment at

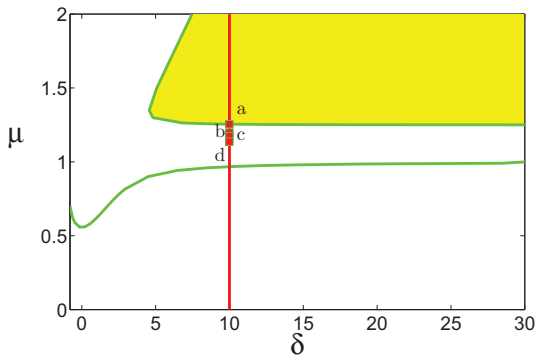

Figure 1. *Bifurcation diagram of the equilibrium at the origin for $\lambda = 0.25$. The yellow region is where the origin is stable and no oscillations are present (death of oscillation area). The upper green curve is the first Hopf bifurcation (supercritical), where the origin loses its stability, and the lower one is a second Hopf bifurcation for the already unstable equilibrium. The red vertical segment is the route that we will take to look for further structure in the diagram.*

$\mu = 1$). The curve in this degenerate case is a curve of double Hopf bifurcation where the two pairs of eigenvalues cross with nonzero velocity at the same time. In this case, the emanating solution is a torus if no resonances are present. We will discuss later in this section the role of tori in the dynamics. For $\lambda \neq 0$ we have analytically proved that the two Hopf curves do not intersect and that each bifurcation curve involves the same pair of eigenvalues all the way.

The outcome of this equilibrium analysis is that outside the yellow region in the upper right corner the system is in a state of oscillatory behavior, but we still have to determine whether or not we should call it synchronized. In [16] the unbounded horizontal strip below the first Hopf bifurcation was termed the *broadband synchronization region*.

The next step in our search for global understanding of the dynamics in this oscillatory region is to compute the family of periodic solutions that is born at the first Hopf curve as one of the parameters is varied, and trace its stability and possible bifurcation by monitoring the Floquet multipliers. This kind of analysis has to rely on numerical algorithms, and we have made extensive use of AUTO, a well-known and tested continuation code in the dynamical systems community [7, 15].

We have chosen a value of $\delta = 10$ for the $\lambda = 0.25$ diagram, guided by the numerical evidence along the red segment in Figure 1. The resulting bifurcation diagram for the family of periodic solutions is shown in Figure 2, where we plot the norm of the solution as a function of the bifurcation parameter μ. Around $\mu = 1.25$, the origin undergoes the above-mentioned Hopf bifurcation (HB) and heads toward the low coupling region. Along the way we have marked several labels (a–d) corresponding to special solutions that will be referred to throughout the paper. Centered around $\mu = 1$ we find a loop with three changes of stability along the branch.

The first stability change as we follow the branch is a limit point (LP1) around $\mu = 0.9$, where the branch turns back and loses stability and the μ parameter begins to increase its value. The branch is drawn with a dashed line to denote that the corresponding periodic solution is unstable (and therefore not observable in simulations) until it reaches a second

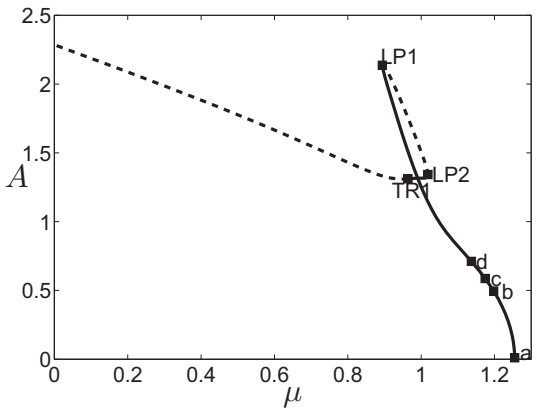

Figure 2. *One-parameter bifurcation diagram as μ varies along the red segment in Figure 1 for $\lambda = 0.25$ and $\delta = 10$. The vertical axis is the norm of the solution. The branch emanates from the origin at a standard supercritical Hopf bifurcation with its usual local square root shape for the amplitude. Labels* a–d *are stable periodic solutions. A first limit point (LP1) is found at $\mu \sim 0.9$, where the branch loses stability. At a second limit point (LP2) the stability is recovered only to be lost again later at a torus bifurcation (TR1). In the interval [LP2, TR1] the system is bistable.*

limit point (LP2), where it recovers the stability and turns back again to decreasing values of μ. The branch of periodic solutions is drawn with a solid line until it reaches a bifurcation point where the stability is lost again in what is called a torus bifurcation (TR1), where a pair of Floquet multipliers leaves the unit circle with a nonvanishing imaginary part. The surviving unstable main branch heads toward the uncoupled limit. Note that, in this case, within the μ interval $[LP2,\ TR1]$ the system is bistable. It is important to note that the relative position of these three bifurcations (two LPs and a TR) varies with δ and really determines the lower border of the region where stable periodic orbits exist in the δ-μ diagram. In a numerical simulation (as in [16]), the observed solution would depend on the initial condition and the basin of attraction of the different solutions. However, if we were aware of this multistability situation, we could determine the basins of attraction of both stable limit cycles, as shown in [38].

The next step in our research is to continue in two parameters this special solution, namely the locus in the δ-μ plane of the two LPs and the TR. We have done this with the help of AUTO, and the results are three more curves in the bifurcation diagram displayed in panel (a) of Figure 3. The point of contact of these tongues with the $\mu = 0$ axis could be predicted just by computing the ratio of the uncoupled periods of the limit cycle of the two Van der Pol oscillators. The synchronization tongues act as bridges of periodic orbits between the $\mu = 0$ limit and the broadband synchronization region.

We display three tongues of 1:k synchronized states bordered by curves of limit points of periodic orbits. The leftmost green tongue centered on $\delta = 0$ corresponds to a 1:1 state, the central blue one is the 1:3 synchronized state explained in Figure 2, and the narrow rightmost black tongue corresponds to a 1:5 resonance. The solid magenta curve is the locus of torus bifurcation of periodic orbits. Figures 3(b) and 3(c) zoom in on the upper part of the tongues to highlight the interaction between the torus bifurcation and the presence of a cusp of limit

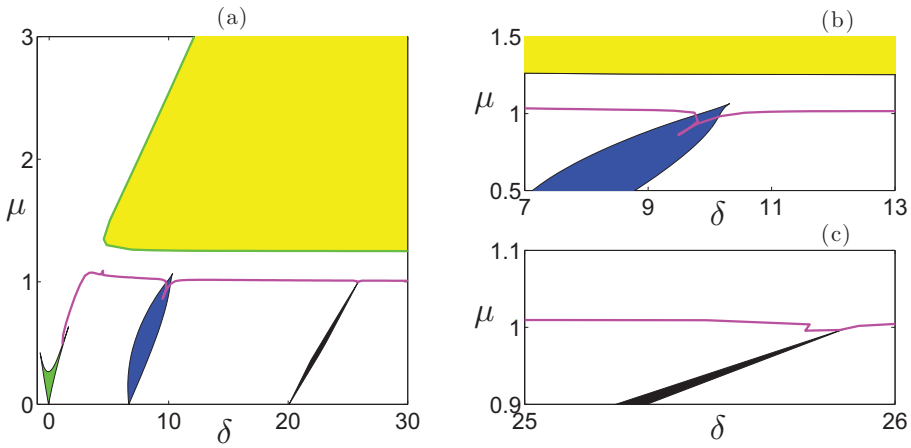

Figure 3. (a) *Two-parameter (δ-μ) continuation of the bifurcation of periodic orbits for fixed $\lambda = 0.25$. We display three tongues of 1:k synchronized states bordered by curves of limit points of periodic orbits. The leftmost green tongue corresponds to a* 1:1 *state, the central blue tongue is the* 1:3 *synchronized state explained in Figure* 2*, and the narrow rightmost tongue corresponds to a* 1:5 *resonance. These tongues are only a subset of the full* 1:k *synchronization region. The magenta solid curve is the locus of torus bifurcation of periodic orbits. Subfigures* (b) *and* (c) *zoom in close to the upper part of the tongues to highlight the interaction between the torus bifurcation and the presence of a cusp of limit points of periodic orbits for $k = 3$ and $k = 5$, respectively.*

points of periodic orbits for $k = 3$ and $k = 5$, respectively. We will later show that there is even finer structure around these bifurcations.

Based on these two parameter continuations, we can identify the borders of the synchronization regions: the upper part of the region is bordered by a supercritical Hopf bifurcation, and the lower part is bordered by a torus bifurcation except where the 1:k tongues appear and connect the so-called broadband synchronization with the uncoupled case ($\mu = 0$).

At this point a comment is in order: we are following periodic orbits that, under our working definition of synchronization, are in the 1:k synchronized state, but as mentioned in section 1, if we would enforce that the dynamics should take place on the surface of a torus in the continuation path, we would certainly obtain other regions and shapes of synchronization. For instance, in our results we would probably include regions where a third harmonic component could present in the time evolution of the orbit that an alternative definition would probably rule out. However, within our definition of synchronization (which agrees with that of [16] and other authors), the continuation and bifurcation results provide valuable insight into the different regions in parameter space.

A systematic analysis of the bifurcation behavior of the branch of periodic orbits that emanates from the Hopf curve reveals further structure within the tongues, namely, the appearance of isolas of periodic orbits detached from the main branch, as shown in Figure 4.

The panels on the left, i.e., (a), (c), (e), are one-parameter bifurcation diagrams, whereas those on the right, i.e., (b), (d), (f), are two-parameter bifurcation sets. Panel (a) corresponds to a bifurcation diagram as μ is varied for fixed $\delta = 9.492$, (c) is for $\delta = 9.4917$, and (e) is for $\delta = 9.0$. We have included a zoom around the "neck" of the loop to highlight the interaction among the different curves of bifurcation. In the right-hand panels the curves of saddle nodes

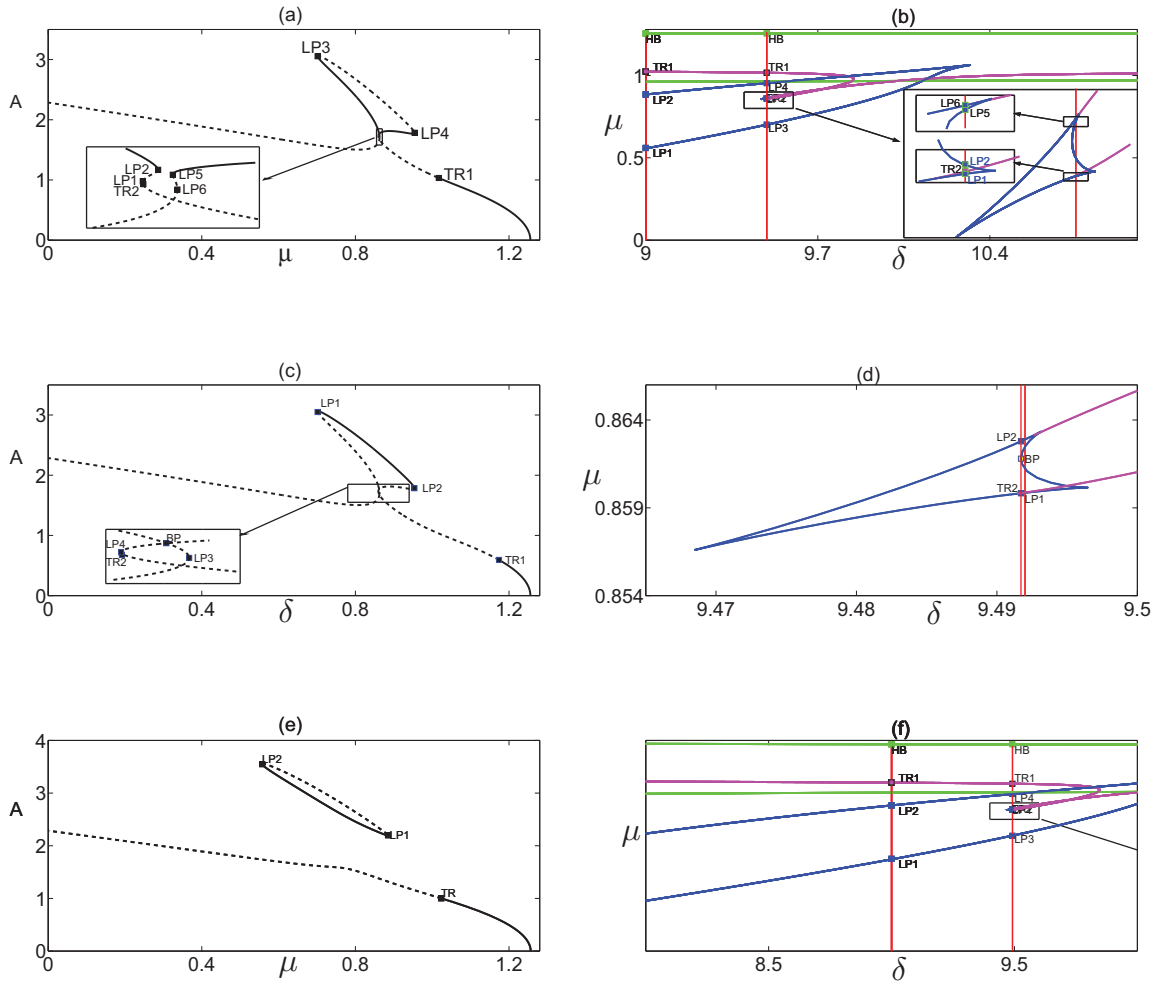

Figure 4. *Formation of an isola of periodic orbits within the synchronization tongues. The panels on the left (*(a), (c), (e)*) are one-parameter bifurcation diagrams, whereas those on the right (*(b), (d), (f)*) are two-parameter bifurcation sets. Panel* (a) *corresponds to* $\delta = 9.492$, (c) *is for* $\delta = 9.4917$, *and* (e) *is for* $\delta = 9.0$. *We have included a zoom around the "neck" of the loop to highlight the interaction among the different curves of bifurcation. Also note that the curve of tori is connected to a swallow-tail curve of saddle nodes of periodic orbits (panels* (b) *and* (d)*). In the right-hand panels the curves of saddle nodes of periodic orbits inside the synchronization tongue are depicted in blue and exhibit a swallow-tail shape, the curves of torus bifurcations are black, and the green lines correspond to the Hopf bifurcation of the equilibrium.*

of periodic orbits inside the synchronization tongue are depicted in blue and exhibit a swallow-tail shape, the curves of torus bifurcations are magenta, and the green lines correspond to the Hopf bifurcation of the equilibrium. The vertical red lines indicate the position of the one-parameter bifurcation curves.

As δ is diminished, the isola is born precisely when the two limit points LP2 and LP5 in the zoom of Figure 4(a) collide and are detected as a branch point (BP) where a branch of nonsymmetric solutions will be born. In Figure 4(d) this corresponds to the tangency of the red segment with one of the sides of the swallow tail. For even lower values of δ as in Figure

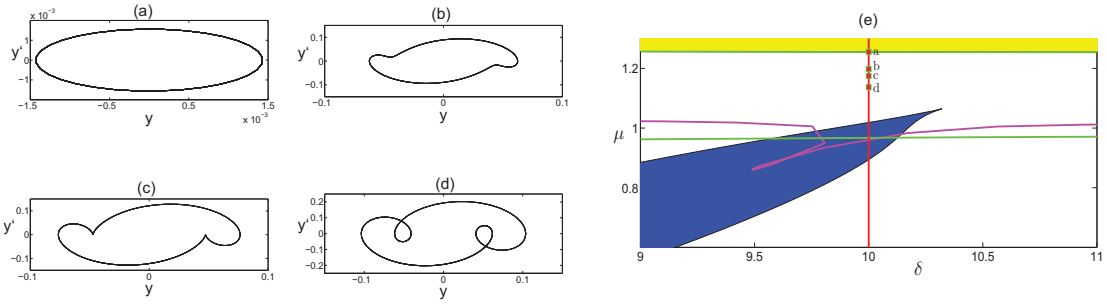

Figure 5. *The onset of the synchronized state reveals the structure of the degraded top. Panel* (e) *is a zoom of the partial bifurcation diagram, Figure* 3(a)*, for* $\lambda = 0.25$*, displaying part of the synchronization tongue in blue, the region of death of oscillations in yellow, the Hopf curves in green, and the curve of torus bifurcations in magenta. The red segment is the route toward the synchronization region.* (a)–(d) *are the* y-$\dot{y}$ *projections of orbits along the family of periodic orbits born at the first Hopf bifurcation at a fixed value of* $\delta = 10$ *and decreasing values of* μ*.* (a) *is a small circular periodic orbit close to the HB (*$\mu = 1.25494$*),* (b) *is for* $\mu = 1.9777$*, where the lobe is starting to appear,* (c) *is the onset of* 1:3 *synchronization for* $\mu = 1.17460$*, and* (d) *is inside the* 1:3 *synchronization region for* $\mu = 1.13711$*. The points* a–d *in panel* (e) *were also shown in Figure* 2*.*

4(e), the isola is completely detached from the main branch and bordered by two limit points of periodic orbits (labeled by LP1 and LP2).

The left-hand panel (a) is the one-parameter bifurcation diagram at a slightly lower value of the frequency mismatch $\delta = 9.5$ before the red segment in Figure 1. The branch of stable periodic orbits is born at a supercritical Hopf bifurcation (HB), undergoes a torus bifurcation (TR) where the stability is lost, and recovers the stability again at a torus bifurcation where the pinching of the loop takes place. If we decrease δ further as in the right-hand panel (b), for $\delta = 9.45$ the loop completely detaches and we have an isola of periodic orbits with a lower part of stable periodic orbits (solid line) and an upper part with unstable periodic orbits (dashed line). The isola is bordered by two limit points, where the stable and unstable subbranches merge and the whole object can be continued in δ and μ. Note that the isolas are within the synchronization tongues of Figure 3.

3.1. The degraded top.

In the previous section we used the term 1:k synchronized state without an explicit comment on how to determine or measure the synchronization itself. We know that at the point where the 1:k tongue emanates from the uncoupled case in the neighborhood of the $\mu = 0$ contact point, the two oscillators have rhythm adjustment and one of the subsystems is rotating k times faster than the other, but it is not clear how far we can get when $\mu > 0$ before this geometrical feature is lost.

In fact, to understand how the system enters in a synchronized state, it is even more instructive to start at the other end of the tongue, more precisely, at the upper Hopf curve, and follow the orbit as we proceed toward lower values of μ, i.e., follow the route a-b-c-d in Figure 2. The shapes of the y-$\dot{y}$ projections of the orbits at those points are presented in the left-hand panels of Figure 5. In panel (a) we see a round and small orbit, as predicted by Hopf's theorem, that starts to develop a lobe, as shown in (b) for lower values of μ. At label c the lobe touches *tangentially* the horizontal axis at $\dot{y} = 0$. At a lower value of μ as in panel (d), the lobe (which is now a loop) drops below the $\dot{y}$ axis. At this point the subsystem y is

performing three revolutions, while the subsystem x performs only one revolution (not shown in the figure); i.e., the coupled system at (d) is in the 1:3 synchronized state, and the tangency shown in panel (c) can be considered as the onset of 1:3 synchronization. Note that the orbits cross the $\dot{y} = 0$ axis six times (three times in each direction) for a 1:3 synchronized state.

Incidentally, we should remark that all of the solutions along the route exhibit an inversion orbital symmetry around the origin inherited from the Van der Pol system (2.1) which consists of the change $y \to -y$ and $x \to -x$ without altering the time. The coupling term does not destroy this symmetry if the transformation is performed simultaneously on the x and y variables.

It is worth noting that all of these geometrical changes still occur far from the proper synchronization tongues bordered by limit points (see the distance between point d and the tongue in panel (e)). This means that in the route that starts at the Hopf bifurcation curve toward the tongue the system enters a 1:k synchronized state from the geometrical point of view long before reaching the tongue.

If we want to plot a region of synchronization in the δ-μ plane, we have to enlarge the blue region outside the tongue. This phenomenon was noticed numerically by the authors of [16] and given the name of *degraded top*. The origin of that name is that geometrically it resembles a triangle-shaped hat on top of the tongue.

In fact, we can affirm that with the geometrical definition of synchronization of [16], the synchronized transition in this region would not be a bifurcation and would not involve a change of stability or new solutions; it is rather a *geometrical feature* (the tangency) that determines the appearance of the synchronized state.

Although synchronization and oscillator suppression may, in many ways, be difficult to distinguish in practice, they are two very different phenomena. Synchronization arises from the quasi-periodic state through a saddle-node bifurcation on the surface of a torus and involves the simultaneous generation of an unstable periodic orbit. Oscillator suppression involves the unilateral suppression of the weaker oscillator and requires a reverse torus bifurcation in which the torus disappears completely.

Note that the geometrical condition does not necessarily correlate with the stability. The system could be entering the synchronized state, but the orbit itself could be unstable, which would make the transition unobservable.

The lesson we learn is that in order to have a 1:k synchronized observable state, we need to fulfill two necessary conditions simultaneously: the orbit must be *stable*, and we must have crossed the tangency condition curve so that the loop crosses the axis more than twice.

It would be very useful to detect the tangency condition and to be able to trace it in the δ-μ plane, as this would indicate the border that would limit the synchronized state from above. Although it is not a bifurcation and no standard test function can be used to characterize it, we will set up an appropriate boundary value problem that is suitable for numerical continuation as follows:

$$\left\{\begin{array}{l} x' = Tx_1, \\ y' = Ty_1, \\ x_1' = T[(1+\lambda-x^2)x_1 - x - \mu(x_1 - y_1)], \\ y_1' = T[(1-y^2)y_1 - (1+\delta)y - \mu(y_1 - x_1)], \end{array}\right. \tag{3.1}$$

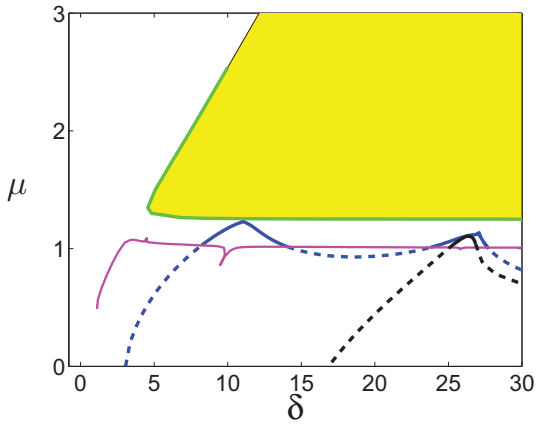

Figure 6. *Two-parameter curves of tangency conditions that border from above the synchronization regions for $k = 3$ (blue) and $k = 5$ (black). The solid and dashed lines denote stability and instability, respectively.*

with the boundary conditions

$$\begin{cases} x(0) = x(1), \\ x_1(0) = x_1(1), \\ y(0) = y(1), \\ y_1(0) = y_1(1), \\ y'(0) = 0, \\ y_1'(0) = 0, \end{cases} \tag{3.2}$$

where we have introduced two auxiliary variables $x_1 = \dot{x}$ and $y_1 = \dot{y}$ to write the second order ODE system (2.1) as a four-dimensional first order system of ODEs, and have scaled the time so that the period of the solution appears explicitly as a parameter and the time interval is $[0, 1]$. The prime denotes the derivative with respect to this scaled time (see [7, 15] for a complete treatment of the continuation method).

The first four boundary conditions impose periodicity on the solution, whereas the fifth is just to establish a time origin and ensure that at time zero we have zero velocity and avoid the phase shift playing a role equivalent to that of the Poincaré phase condition in the standard continuation of periodic orbits. The last boundary condition is the crucial one and imposes the geometrical *tangency* condition of the lobe at the beginning (and at the end due to the periodicity) of the orbit.

The starting point for the 1:3 tangency threshold continuation is the orbit shown in Figure 5(b).

The boundary value problem (3.1), (3.2) is well posed, and the number of free parameters is equal to the number of boundary conditions minus the dimension of the system plus one; in our case, $n_{par} = n_{bc} - n + 1 = 6 - 4 + 1 = 3$. These three parameters will be δ, μ, and T, which, in general, will change along the curve.

The results of this continuation are shown in Figure 6 for $k = 3$ (blue curve) and $k = 5$ (black curve). For the latter case we have followed another route to the synchronization tongues for $\delta = 26.2409$ and located a second tangency for $\mu = 1.10433$. The solid or dashed

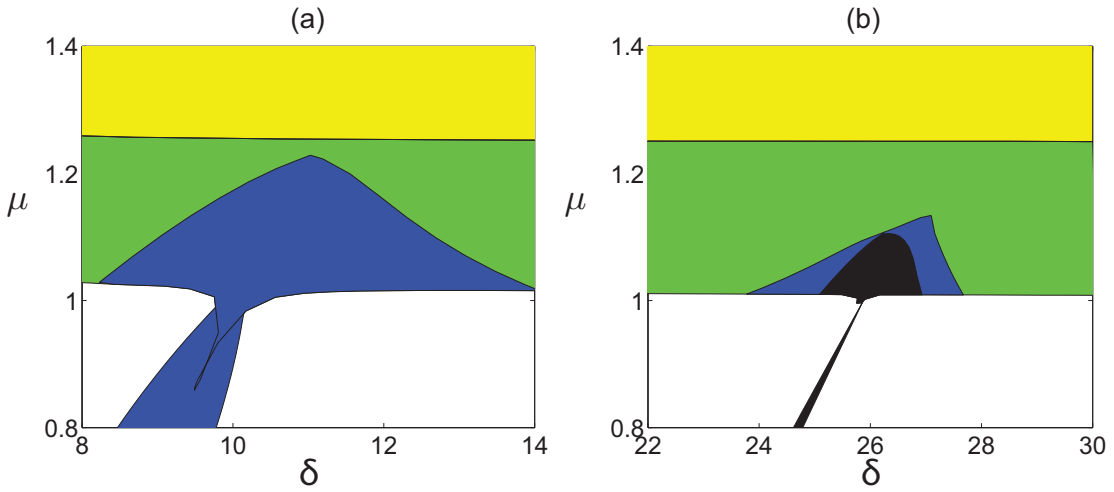

Figure 7. *The structure of the degraded top for $k = 3$ (a) and $k = 5$ (b). The blue region corresponds to the* 1:3 *resonance, whereas the black one corresponds to the* 1:5. *The pointed form of the resonance tongue in Figure* 5 *is no longer present because it has been enlarged by the degraded top. Note that, as expected, the $k = 5$ region is narrower than the $k = 3$ region.*

line denotes the stability of the solution and, as discussed above, does not depend on the tangency but on the fact of having crossed the torus or limit point curves. The points of contact between the $k = 3$ and $k = 5$ curves could be tricky and have to be numerically analyzed with care.

Above these curves the tangency has still not occurred, and, consequently, the system is still not in the synchronized state. On the other hand, as soon as we step into the other side of the curve, the lobe drops below the $\dot{y} = 0$ axis and two new crossings appear. Note that if the orbit is symmetrical, a twin lobe and crossings develop at the other side of the origin.

Figure 7 shows the new synchronization region that we have explained with the boundary value tangency continuation. The pointed form of the resonance tongue of Figure 5 is no longer present, as it has been enlarged by the degraded top. For this value of λ it is a triangle-shaped region not connected to the Hopf curve, surrounded from above by the tangency condition and from below by a torus bifurcation curve. Precisely where this torus curve develops a cusp-like structure the synchronization tongue bordered by limit points of periodic orbits penetrates into the new region. This compound synchronization region is what the authors of [16] called the *degraded top*. We have followed this region for different values of λ, and the tangency border itself develops additional structure; a detailed analysis will be published elsewhere.

The continuation of this tangency condition identifies the upper border of the synchronized region and the corresponding route to synchronization.

3.2. Even k synchronization tongues. In previous sections we have described and characterized the synchronization tongues corresponding to odd values of k (see Figure 3) that were born at the $\mu = 0$ line. As this uncoupled case consists of two attracting limit cycles, the resulting tori are hyperbolic and, generically, persistent under small perturbations. This means that we would also expect to find even k tongues.

However, with our numerical procedure that starts with a branch of periodic orbits at the upper Hopf curve and the location of a limit point bifurcation, or with the extensive numerical scanning of the authors of [16], initially no traces of them were found.

In this section we present a simple symmetry-based argument that explains why this is the case if we do not include some symmetry-breaking solutions in our search. We will show how the combined symmetry of the four-dimensional system (2.1) inherited from the symmetry of each separate Van der Pol oscillator forces the parity of k to be odd for symmetrical periodic solutions.

Let us consider two symmetry operators S_x and S_y that actuate only on one of the subsystems by changing the sign of the x or y variable, respectively, without altering the time variable. The combination of both operators is another symmetry, $S = S_x S_y$. It is evident that for $\mu = 0$ the system (2.1) is both S_x and S_y symmetric, and consequently it is also S symmetric.

The geometrical interpretation of this S operator is that for symmetrical periodic solutions we can reconstruct the whole orbit by knowing just half of it. If T is the period of the orbit and $u(t) = (x(t), \dot{x}(t), y(t), \dot{y}(t))$ is the state, then for any time t, the following relation holds:

$$u\left(t + \frac{T}{2}\right) = Su(t). \tag{3.3}$$

Furthermore, for $\mu = 0$ the symmetric solution $u(t) = (x(t), \dot{x}(t), y(t), \dot{y}(t))$ at a p:q resonance (with $\gcd(p, q) = 1$), where the bifurcating in the μ solution performs p full revolutions in subsystem x, whereas the subsystem y performs q full cycles, satisfies

$$u\left(t + \frac{T}{2}\right) = S_x^p S_y^q u(t). \tag{3.4}$$

However, for $\mu \neq 0$ the coupling term mixes the x and y variables, and S_x and S_y acting independently are *not* symmetries of the system; only S retains this property in the coupled region.

The symmetry relation (3.4) can persist for $\mu \neq 0$ only in the case that $S_x^p S_y^q = S$, that is, when both p and q are odd. For the 1:k resonance this means that k has to be necessarily odd.

Consequently, a forced symmetry-breaking bifurcation happens as soon as $\mu \neq 0$ for even values of k. This implies that in order to locate the new unsymmetrical synchronization tongues for even values of k the periodic orbits have to undergo a pitchfork or symmetry-breaking bifurcation.

If we return our attention to Figure 4(d), we have already found one of those bifurcations while analyzing the appearance of isolas. From this bifurcation point it is possible to launch and continue a family of nonsymmetrical periodic solutions that allowed us to locate even k tongues halfway between any of the two consecutive odd k tongues. In Figure 8 we present the final bifurcation diagram of the coupled Van der Pol oscillators (2.1) for $\lambda = 0.25$, including the even k tongues. This new structure completes the bifurcation diagram in a consistent and appealing way. The narrow red tongue between the green symmetric $k = 1$ and the blue symmetric $k = 3$ tongues corresponds to the *nonsymmetrical* $k = 2$. The same holds for the

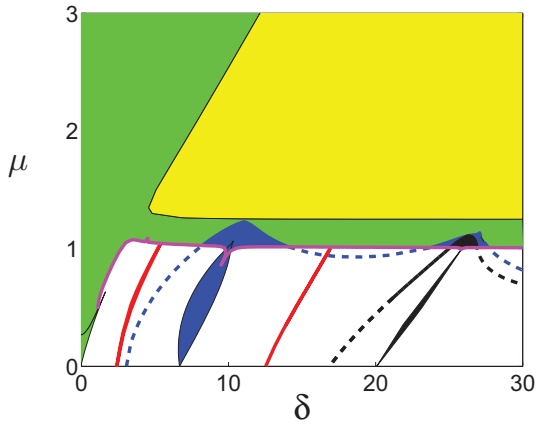

Figure 8. *Complete two-parameter bifurcation diagram including the nonsymmetric even k tongues. The narrow black tongue corresponds to the nonsymmetrical $k = 2$, the green region corresponds to symmetric $k = 1$, and the blue tongues correspond to symmetric $k = 3$.*

red $k = 4$ tongue. Note that only the narrowness of the $k = 2$ and $k = 4$ tongues is still not well understood, and, probably, a full theoretical symmetry bifurcation analysis is needed to understand this nongeneric behavior.

4. Conclusions. We have undertaken a bifurcation analysis of a velocity coupled system of two classical nonidentical Van der Pol oscillators to understand the appearance and structure of 1:k parameter regions with synchronized states as we vary the coupling and the frequency mismatch. These regions include multistability of solutions and are formed by classical tongues bordered by curves of limit point bifurcation of periodic orbits with isola structure and an additional subregion surrounded by curves of torus bifurcations and a curve characterized by a geometrical tangency condition. Symmetry arguments explain the difference between the even and odd k cases.

The bifurcation approach undertaken in this work could be extended by continuing the families of tori and their bifurcations with the techniques of [28] to try to further clarify the interaction between tori and limit points of periodic orbit bifurcations. The extension of this result to other values of λ and to the negative μ and δ parameters is deferred to future work.

Acknowledgments. The authors acknowledge fruitful discussions with E. Freire, S. Wieczorek, F. Schilder, and E. Doedel and especially thank A. Vanderbauwhede for assistance with the symmetry explanation of the difference between even and odd values of k. They would also like to thank an anonymous referee for greatly improving the manuscript in the review process.

REFERENCES

[1] J. K. Aggarwal and C. G. Richie, *On coupled van der Pol oscillators*, IEEE Trans. Circuit Theory, 13 (1966), pp. 465–466.

[2] D. G. Aronson, G. B. Ermentrout, and N. Kopell, *Amplitude response of coupled oscillators*, Phys. D, 41 (1990), pp. 403–449.

[3] A. Balanov, N. Janson, D. Postnov, and O. Sosnovtseva, *Synchronization. From Simple to Complex*, Springer-Verlag, Berlin, 2009.
[4] M. A. Barrón and M. Sen, *Synchronization of four coupled van der Pol oscillators*, Nonlinear Dynam., 56 (2010), pp. 357–367.
[5] R. Brown and L. Kocarev, *A unifying definition of synchronization for dynamical systems*, Chaos, 10 (2000), pp. 344–349.
[6] E. Camacho, R. Rand, and H. Howland, *Dynamics of two van der Pol oscillators coupled via a bath*, Internat. J. Solids Structures, 41 (2004), pp. 2133–2143.
[7] E. J. Doedel, A. R. Champneys, T. F. Fairgrieve, Y. A. Kuznetsov, B. Sandstede, and X. J. Wang, *AUTO97: Continuation and Bifurcation Software for Ordinary Differential Equations*, http://indy.cs.concordia.ca (1997).
[8] A. M. dos Santos, S. Lopes, and R. L. Viana, *Rhythm synchronization and chaotic modulation of coupled van der Pol oscillators in a model for the heartbeat*, Phys. A, 338 (2007), pp. 335–355.
[9] G. B. Ermentrout, *Oscillator death in populations of "all to all" coupled nonlinear oscillators*, Phys. D, 41 (1990), pp. 219–231.
[10] J. Guckenheimer and P. Holmes, *Nonlinear Oscillations, Dynamical Systems and Bifurcation of Vector Fields*, Springer-Verlag, New York, 2002.
[11] P. J. Holmes and R. H. Rand, *Bifurcation of the forced van der Pol oscillator*, Quart. Appl. Math., 35 (1977/78), pp. 495–509.
[12] V. Jovanovic and S. Koshkin, *Synchronization of Huygens' clocks and the Poincaré method*, J. Sound Vibration, 331 (2012), pp. 2887–2900.
[13] R. Katoh and M. Mori, *Control method of biped locomotion giving asymptotic stability of trajectory*, Automatica J. IFAC, 20 (1984), pp. 405–414.
[14] T. Kawahara, *Coupled Van der Pol oscillators—A model of excitatory and inhibitory neural interactions,* Biol. Cybern., 39 (1980), pp. 37–43.
[15] B. Krauskop, H. Osinga, and J. Galán-Vioque, *Numerical Continuation Methods for Dynamical Systems: Path Following and Boundary Value Problems*, Springer-Verlag, Berlin, 2007.
[16] A. P. Kuznetsov and J. Roman, *Properties of synchronization in the systems of non-identical coupled van der Pol and van der Pol-Duffing oscillators. Broadband synchronization*, Phys. D, 238 (2009), pp. 1499–1506.
[17] S. P. Kuznetsov and I. R. Sataev, *Hyperbolic attractor in a system of coupled non-autonomous van der Pol oscillators: Numerical test for expanding and contracting cones*, Phys. Lett. A, 365 (2007), pp. 97–104.
[18] Y. A. Kuznetsov, *Elements of Applied Bifurcation Theory*, Springer-Verlag, New York, 2004.
[19] X. Li, J. C. Ji, and C. H. Hansen, *Dynamics of two delay coupled van der Pol oscillators*, Mech. Res. Comm., 33 (2006), pp. 614–627.
[20] D. A. Linkens, *The stability of entrainment conditions for RLC coupled van der Pol oscillators used as a model for intestinal electrical rhythms*, Bull. Math. Biol., 39 (1977), pp. 359–372.
[21] E. Mosekilde, R. Feldberg, C. Knudsen, and M. Hindsholm, *Mode locking and spatiotemporal chaos in periodically driven Gunn diodes*, Phys. Rev. B, 41 (1990), pp. 2298–2306.
[22] I. Pastor-Díaz and A. López-Franguas, *Dynamics of two coupled van der Pol oscillators*, Phys. Rev. E, 52 (1995), pp. 1480–1489.
[23] A. Pikovsky, M. Rosenblum, and J. Kurths, *Synchronization, a Universal Concept in Nonlinear Sciences*, Cambridge University Press, New York, 2001.
[24] R. H. Rand and P. J. Holmes, *Bifurcation of periodic motions in two weakly coupled van der Pol oscillators*, Internat. J. Non-Linear Mech., 15 (1980), pp. 387–399.
[25] B. Rasmussen, *Numerical Methods for the Continuation of Invariant Tori*, Ph.D. thesis, School of Mathematics, Georgia Institute of Technology, Atlanta, GA, 2003.
[26] K. Rompala and R. Rand, *Dynamics of three coupled van der Pol oscillators with application to circadian rhythms*, Commun. Nonlinear Sci. Numer. Simul., 12 (2007), pp. 794–803.
[27] G. Saxena, A. Prasad, and R. Ramaswamy, *Amplitude death: The emergence of stationarity in coupled nonlinear systems*, Phys. Rep., 521 (2012), pp. 205–228.
[28] F. Schilder, H. M. Osinga, and W. Vogt, *Continuation of quasi-periodic invariant tori*, SIAM J. Appl. Dyn. Syst., 4 (2005), pp. 459–488.

[29] D. W. Storti and R. H. Rand, *Dynamics of two strongly coupled van der Pol oscillators*, Internat. J. Non-Linear Mech., 17 (1982), pp. 143–152.
[30] S. H. Strogatz, *Nonlinear Dynamics and Chaos: With Applications to Physics, Biology, Chemistry, and Engineering*, Perseus Books, Cambridge, MA, 2000.
[31] J. Sturis, C. Knudsen, N. M. O'Meara, J. S. Thomsen, E. Mosekilde, E. Van Cauter, and K. S. Polonsky, *Phase-locking regions in a forced model of slow insulin-glucose oscillations*, Chaos, 5 (1995), pp. 193–199.
[32] M. A. Taylor and I. G. Kevrekidis, *Some common dynamic features of coupled reacting systems*, Phys. D, 51 (1991), pp. 219–231.
[33] M. A. Taylor and I. G. Kevrekidis, *Couple, double, toil and trouble: A computer assisted study of two coupled CSTRs*, Chem. Eng. Sci., 48 (1993), pp. 2129–2149.
[34] B. van der Pol, *A theory of the amplitude of free and forced triode vibrations*, Radio Rev., 1 (1920), pp. 701–710.
[35] B. van der Pol and J. van der Mark, *Frequency demultiplication*, Nature, 120 (1927), pp. 363–364.
[36] B. van der Pol and J. van der Mark, *The heartbeat considered as a relaxation oscillation, and an electrical model of the heart*, Phil. Mag. Suppl., 6 (1928), pp. 763–775.
[37] W. Vance and J. Ross, *A detailed study of a forced chemical oscillator: Arnol'd tongues and bifurcation sets*, J. Chem. Phys., 91 (1989), pp. 7654–7670.
[38] J. Xu, R. S. Guttalu, and C. S. Hsu, *Domains of attraction for multiple limit cycles of coupled van der Pol equations by simple cell mapping*, Internat. J. Non-Linear Mech., 20 (1985), pp. 507–517.
[39] R. Yamapi and P. Woafo, *Dynamics and synchronization of coupled self-sustained electromechanical oscillators*, J. Sound Vibration, 285 (2005), pp. 1151–1170.